Precipitation comparison for the CFSR, MERRA, TRMM3B42 and Combined Scheme datasets in Bolivia

Luis A. Blacutt [a,*], Dirceu L. Herdies [a], Luis Gustavo G. de Gonçalves [a], Daniel A. Vila [a], Marcos Andrade [b]

[a] Centro de Previsão de Tempo e Estudos Climáticos/Instituto Nacional de Pesquisas Espaciais (CPTEC/INPE), Cachoeira Paulista, SP 12630-000, Brazil
[b] Laboratorio de Física de la Atmósfera – Instituto de Investigaciones Físicas – Universidad Mayor de San Andrés (LFA-IIF-UMSA) Campus Universitario Cota Cota calle 28 Edificio Facultativo p.2 Casilla 8635, Bolivia

ABSTRACT

An overwhelming number of applications depend on reliable precipitation estimations. However, over complex terrain in regions such as the Andes or the southwestern Amazon, the spatial coverage of rain gauges is scarce. Two reanalysis datasets, a satellite algorithm and a scheme that combines surface observations with satellite estimations were selected for studying rainfall in the following areas of Bolivia: the central Andes, Altiplano, southwestern Amazonia, and Chaco. These Bolivian regions can be divided into three main basins: the Altiplano, La Plata, and Amazon. The selected reanalyses were the Modern-Era Retrospective Analysis for Research and Applications, which has a horizontal resolution (~50 km) conducive for studying rainfall in relatively small precipitation systems, and the Climate Forecast System Reanalysis and Reforecast, which features an improved horizontal resolution (~38 km). The third dataset was the seventh version of the Tropical Rainfall Measurement Mission 3B42 algorithm, which is conducive for studying rainfall at an ~25 km horizontal resolution. The fourth dataset utilizes a new technique known as the Combined Scheme, which successfully removes satellite bias. All four of these datasets were aggregated to a coarser resolution. Additionally, the daily totals were calculated to match the cumulative daily values of the ground observations. This research aimed to describe and compare precipitations in the two reanalysis dataset, the satellite-algorithm dataset, and the Combined Scheme with ground observations. Two seasons were selected for studying the precipitation estimates: the rainy season (December–February) and the dry season (June–August). The average, bias, standard deviation, correlation coefficient, and root mean square error were calculated. Moreover, a contingency table was generated to calculate the accuracy, bias frequency, probability of detection, false alarm ratio, and equitable threat score.

All four datasets correctly depicted the spatial rainfall pattern. However, CFSR and MERRA overestimated precipitation along the Andes' eastern-facing slopes and exhibited a dry bias over the eastern Amazon; TRMM3B42 and the Combined Scheme depicted a more realistic rainfall distribution over both the Amazon and the Andes. When separating the precipitation into classes, MERRA and CFSR overestimated light to moderate precipitation (1–20 mm/day) and underestimated very heavy precipitation (>50 mm/day). TRMM3B42 and CoSch depicted behaviors similar to the surface observations; however, CoSch underestimated the precipitation in very intense systems (>50 mm/day).

The statistical variables indicated that CoSch's correlation coefficient was highest for every season and basin. Additionally, the bias and RMSE values suggested that CoSch closely represented the surface observations.

1. Introduction

Precipitation knowledge is relevant to many applications: it affects our ability to determine and understand the hydrological balance, it helps improve water management in both agriculture and power generation, and it is needed for studies on drought relief and flood awareness. Overall, precipitation knowledge is important for critical social and climatological issues.

A large amount of global precipitation occurs in the tropics, where it is susceptible to variations related to climatic events, such as El Nino–Southern Oscillation. Describing precipitation is complicated, as it is variable at a small scale and is highly non-normally distributed (Huffman et al., 2007).

The Bolivian region features several characteristics that influence the temporal and spatial characteristics of precipitation. Geomorphologically, the area is dominated by the Andes Mountains, where the highest elevation is around 6000 m asl. Between 14°S and 22°S, the Andes are divided into two meridional mountain ranges by a high-altitude basin (~4000 m asl) known as the Altiplano. During the summer (December–

* Corresponding author.
E-mail addresses: luis.blacutt@cptec.inpe.br, lblacutt@fiumsa.edu.bo (L.A. Blacutt).

January), moisture from the Amazon is transported to the northwestern region of the continent by the low-level jet (LLJ), which is blocked by the Andes and channeled to the eastern rim of the Andes near Santa Cruz de La Sierra. From there, the moisture moves toward northern Argentina or southeastern Brazil (Nogués-Paegle and Mo, 1997; Herdies et al., 2002). Additionally, the 200-hPa Bolivian High, which is an upper tropospheric anticyclone formed by intense summertime convection and latent heating over the northern Amazon during the summer, is present (Lenters and Cook, 1997, 1999).

Globally, two types of data sources are available for precipitation: surface observations and indirect measurements (e.g., satellite or radar). Surface observations from rain gauges are the only direct measurements; however, they are affected by systematic errors, i.e., losses due to wetting, evaporation, and aerodynamic effects (Nespor and Sevruk, 1999; Porcù et al., 2014). Over South America, the spatial distribution of rain gauges is denser along the main river courses and toward the edge of the continent (de Gonçalves et al., 2006); this distribution may lead to possible biases in regional rainfall estimates (Clarke et al., 2011). Notably, data scarcity is accompanied by another problem, data access reliability, which creates the same scenario, i.e., limited knowledge of the spatial and temporal characteristics of precipitation.

Indirect measurements offer large spatial coverage, but they must be calibrated to obtain meaningful values. Over the past four decades, tremendous effort has been made to monitor and understand precipitating systems from space at first, techniques were developed to estimate precipitation from convection based on infrared channels; then, microwave channels provided an opportunity to estimate precipitation from cloud processes; it became possible to estimate precipitation proxies with the advent of high-frequency polarized channels over terrestrial regions (Arkin and Meisner, 1987; Spencer et al., 1989). Nevertheless, mountainous snow-covered regions presented another challenge. Microwave algorithms failed to estimate precipitation from shallow orographic systems and warm-rain processes (Huffman et al., 1995; Dinku et al., 2010).

The precipitation estimation methods radically changed after the inclusion of a precipitation radar which is an active sensor onboard the Tropical Rainfall Measuring Mission (TRMM), a joint project of the Japan Aerospace Exploration Agency (JAXA) and the U.S. National Aeronautics and Space Administration (NASA) that was launched in 1997 (Kummerow et al., 1998). TRMM improved knowledge of several aspects of the spatio-temporal precipitation distribution, intensity, and vertical structure (Ouma et al., 2012; Liu et al., 2012). However, the absolute accuracy of satellite precipitation data is questionable (Tian and Peters-Lidard, 2010). Recently, JAXA and NASA launched the Global Precipitation Measurement (GPM), which is expected to improve knowledge of precipitation systems (Tapiador et al., 2012; Hou et al., 2013; Smith et al., 2004). Several TRMM rainfall products use algorithms that combine measurements from various sensors.

The TRMM Multi-satellite Precipitation Analysis (TMPA, TRMM3B42 hereafter (Huffman et al., 2007)) is a real-time 3-hourly precipitation estimation algorithm. TRMM3B42 was shown by the International Precipitation Working Group (IPWG) to be an accurate high resolution satellite-based rainfall estimate for operational use to date by in situ continental-scale validation and intercomparison of operational and semi-operational satellite rainfall estimates over Australia, the US and Northwestern Europe (Ebert et al., 2007). The algorithm encounters difficulties over mountainous regions, for example, TRMM has a dry bias over the Colombian highlands (Dinku et al., 2010) and over the Titicaca Lake basin in the Andean Altiplano (Heidinger et al., 2012). However, meaningful information can be extracted from these data to study the diurnal cycle (Johnson et al., 2010). In fact, TRMM3B42 generates the best precipitation estimates for northwestern China as compared with two other products: the Climate Prediction Center's Morphing technique (CMORPH) and a precipitation-estimation method using artificial neural networks (Yang and Luo, 2014).

TRMM3B42 overestimates the total rainfall in Ethiopia, while it underestimates the total rainfall in Colombia (Dinku et al., 2010).

Additionally, TRMM3B42 is incapable of detecting light rainfall amounts and underestimates rainfall in the dry season (Ward et al., 2011). However, during the warm season, TRMM3B42 overestimates intense precipitation (Behrangi et al., 2011).

To characterize precipitation, observational datasets and satellite estimations can be combined to generate a so-called "reanalysis". Reanalysis data generally represent state-of-the-art gridded atmospheric states during specific periods. The data are generated by a model kept constant in time with a constant data assimilation system. The second version of the Climate Forecast System Reanalysis and Reforecast (CFSR hereafter (Saha et al., 2010)) is the most recent model version from the National Center for Environmental Prediction at the National Center for Atmospheric Research (NCEP–NCAR). CFSR is a reanalysis dataset that exhibits improved horizontal (~38 km) and vertical resolutions (64 sigma-pressure hybrid levels), making it possible to perform analyses for precipitating features coming from smaller than of sub-synoptic systems. An analysis of daily precipitation was performed for all seasons over South America: a wet bias was found over the Andes Mountains (Silva et al., 2011). Also, a dry bias was found for the Amazon compared with a ground-based dataset (Quadro et al., 2007). Additionally, an artifact was found in the Andes near the Altiplano region (Eichler and Londoño, 2013).

The second reanalysis dataset used here is the Modern-Era Retrospective Analysis for Research and Application (MERRA), which aimed to improve the hydrological cycle because various aspects of the hydrological cycle were not adequately depicted by previous-generation datasets (Rienecker et al., 2011). Over South America, differences in the parameters that characterize the shape, scale, and tails of the frequency distributions were found (Carvalho et al., 2012). Over the South Atlantic Convergence Zone, precipitation from MERRA was found to closely represent the annual cycle (Quadro et al., 2007) and to underestimate precipitation compared with ground-based data (Quadro et al., 2012).

An alternative approach was recently developed to positively combine the strengths of two precipitation data sources: surface observations and satellite estimations. Surface observations lack spatial and temporal coverage, while satellite estimates exhibit great spatial and temporal coverage but lack absolute accuracy. A scheme to extract their respective advantages can be obtained by appropriately combining rain gauge and satellite estimations (Rozante et al., 2010; Zhao et al., 2012). In particular, Vila et al. (2009) improved satellite estimations by combining additive and ratio biases, which successfully removed the satellite bias for South America.

Despite all the work accomplished to study precipitation over the South American continent, the knowledge about the capabilities and limitations of precipitation products over Bolivia is still poor. The purpose of this study is to assess the capabilities and limitation of four precipitation estimation products to describe rainfall over Bolivia for two different seasons. In this work, the methodology used by Vila et al. (2009) was applied to generate an improved gridded dataset for the Bolivian region, i.e., the Central Andes, Altiplano, and southwestern Amazonia. The results were compared with two reanalyses and a satellite precipitation estimate against surface observations. First, a spatial inspection was performed; then, the statistical analysis parameters were calculated and compared by extracting estimates that correspond to the nearest rain gauge points. This paper is organized as follows: Section 2 describes the relevant datasets; Section 3 describes the results and discusses the capabilities and limitations of each dataset; and Section 4 presents the conclusions.

2. Data and methodology

This study evaluates two reanalyses, i.e., MERRA (Rienecker et al., 2011) and CFSR (Saha et al., 2010), the satellite product TRMM3B42 (Huffman et al., 2007), and a combined product (CoSch) (Vila et al., 2009). These products have different spatial and temporal resolutions

Table 1
Contingency table.

		Gauges		Total
		Yes	No	
Estimated	Yes	Hits	False alarms	Estimated yes
	No	Misses	Correct negatives	Estimated no
Total		Observed yes	Observed no	Total

and periods. In this study, the satellite and reanalysis data were aggregated into 24-h totals (12Z–12Z) for a comparison with the cumulative daily precipitation gauges over the period of 1999–2009. Additionally, the datasets were interpolated to the lowest horizontal resolution (1/ $2° \times 2/3°$). Two seasons were selected to compare and study the precipitation estimates: the rainy season (December–February) and the dry season (June–August). A comparison was performed for the three main Bolivian basins: the Altiplano, La Plata, and Amazon. First, selected pixels were extracted from each dataset corresponding to the nearest surface station, which was an aggregate of 205 surface stations. Therefore, a point-by-point comparison could be performed.

For each basin and season, the comparison includes a climatological description and a statistical description. The climatological description is presented by showing the average daily values for each month and a spatial analysis. The statistical analysis includes quantitative statistics and categorical statistics. For the quantitative statistics, the following parameters were calculated: bias, root mean squared error, and a correlation coefficient; the expressions for these statistics can be found in Wilks (2006).

For the categorical statistics, simple contingency tables were generated by assuming dichotomous verification of the occurrence of an event using a rain gauge; specifically, the event occurs or does not occur, as shown in Table 1 (Ebert et al., 2007). The parameters calculated with the contingency table are as follows: accuracy, frequency bias score, probability of detection (POD), false alarm ratio (FAR), and equitable threat score (ETS, Gilbert skill score). The probability of detection provides the fraction of rain occurrences that were correctly detected (a perfect score is 1), whereas the false alarm ratio (FAR) measures the fraction of rain detections that were actually false alarms (a perfect score is 0). The equitable threat score (ETS) provides a fraction of the observed and/or detected rain that was correctly estimated after adjusting for the number of hits that could be expected purely due to random chance (a perfect score is 1). The ETS is commonly used as an overall skill measure, in which the POD and FAR provide complementary information on biases, misses, and false alarms. The equations to calculate

the aforementioned indexes and complementary explanations can be found on the International Precipitation Working Group web page (IPWG, http://www.isac.cnr.it/~ipwg/validation.html). Similar analysis was performed for Southern South America (Salio et al., 2014).

2.1. Bolivian rain-gauge network

Daily rain gauge data used in our investigations were obtained from the Bolivian Weather Service (Servicio Nacional de Meteorología e Hidrología; SENAMHI in Spanish). The SENAMHI maintains a dataset of more than 300 surface stations (see Fig. 1), 36 of which report regularly to the Global Telecommunications System (GTS). For this study, the number of stations that cover the period of 01 Jan 1999–31 Dec 2009 was reduced to 205. No additional quality checks were performed on these data. The observations were interpreted as 24-h accumulated rainfall at 8 am local time (12Z) on the day of interest.

2.2. Modern-era retrospective analysis for research and applications

MERRA aimed to improve the hydrological cycle in earlier generations of reanalysis. Recently, a new version of MERRA was released (Rienecker et al., 2011) that is based on version 5.2.0 of the Goddard Earth Observing System (GEOS) atmospheric model and data assimilation system Details on the assimilation system are provided in Rienecker et al. (2008). Precipitation assimilation systems include instantaneous rain rate estimates from the Special Sensor Microwave Imager (SSM/I) and the TRMM Microwave Imager (TMI); details are provided in Treadon et al. (2002). The current MERRA reanalysis has an improved spatial resolution of 1/2° latitude and 2/3° longitude, and it is available on an hourly timescale from 1979 to the present.

2.3. Climate forecast system reanalysis

NCEP has recently developed a new generation of reanalysis products as part of the Climate Forecast System Reanalysis and Reforecast (CFSR) project (Saha et al., 2010). Compared with the earlier NCEP reanalysis, three major changes were implemented: 1) the data have higher horizontal and vertical resolutions (an atmospheric horizontal spectral resolution of T382 ≈ 38 km and a vertical resolution of 64 sigma-pressure hybrid levels) and a temporal resolution of 6 h; 2) the guess forecast is generated from a coupled atmospheric–ocean–sea ice–land system; and 3) historical satellite radiance measurements are assimilated. The surface model presents four soil layers, and the atmospheric model assimilates the CO_2, aerosols and other trace gas variations from 1979 to the present.
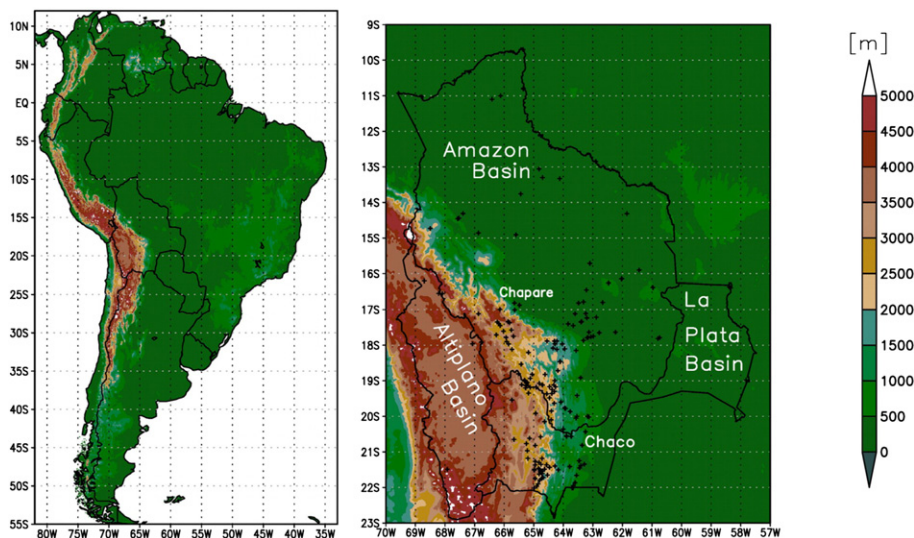

Fig. 1. Geographical location of Bolivia and the characteristic regions used to describe rainfall.

Two datasets are used to generate precipitation fields in CFSR: the pentad Climate Prediction Center (CPC) Merged Analysis of Precipitation (CMAP) and a daily rain-gauge analysis. The precipitation field is generated by blending the two datasets with the CFSR background on 6-hourly global data assimilation of precipitation system. The blending function is latitude dependent, which favors a satellite-based CMAP analysis in the tropics (Xie et al., 2007).

2.4. Version 7 of the TRMM 3B42 algorithm

The seventh research version of the Tropical Rainfall Measuring Mission (hereafter TRMM3B42) relies primarily on passive microwave (PMW) precipitation estimates from the SSM/I, the Special Sensor Microwave Imager and Sounder (SSMIS), the TMI, the Advanced Microwave Sounding Unit (AMSU), the Microwave Humidity Sounder
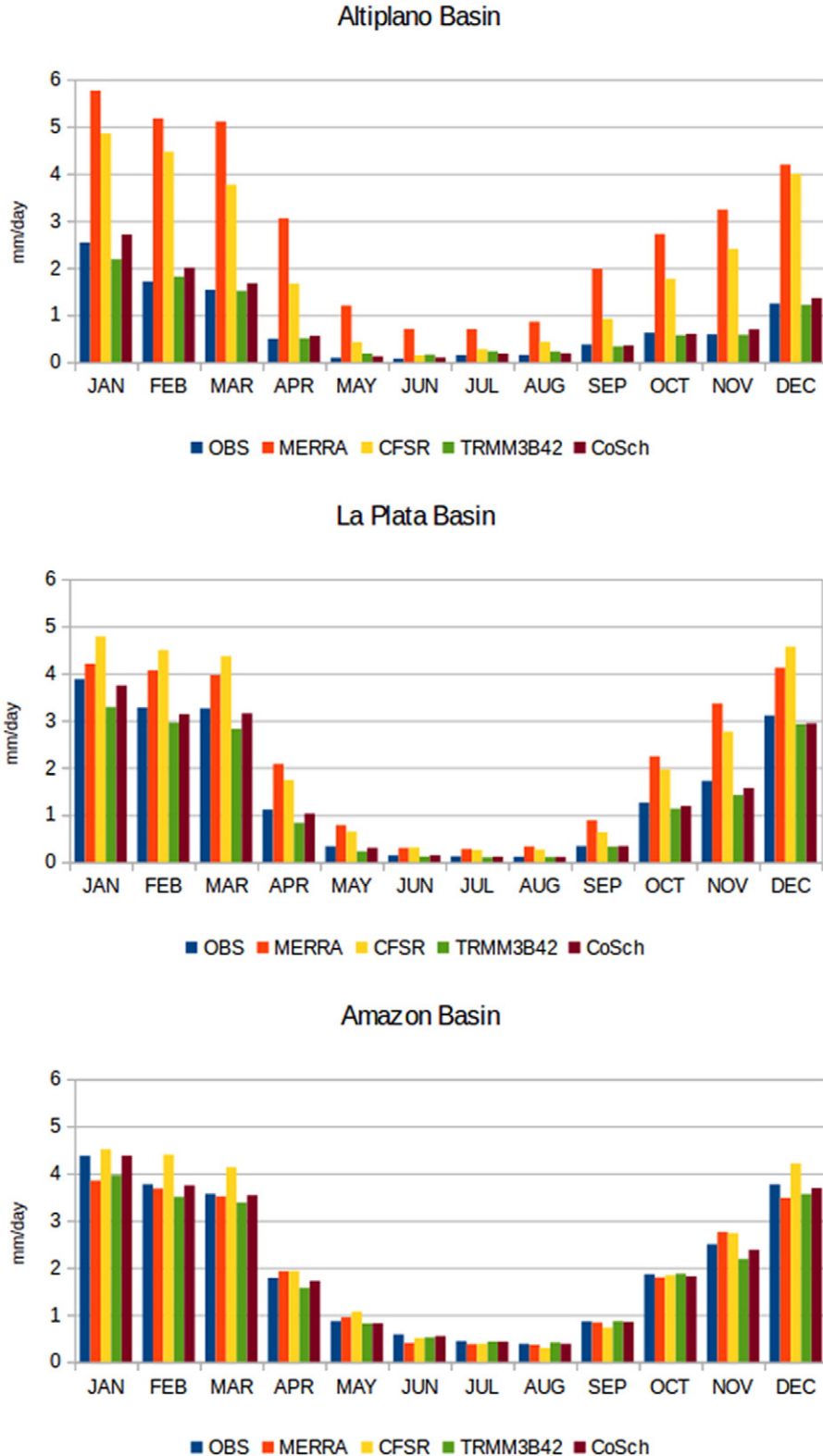

Fig. 2. Average annual precipitation cycle for the 1999–2009 period for each dataset and basin.

(MHS) and the Advanced Microwave Scanning Radiometer for the Earth Observing System (AMSR-E). The PMW data were first calibrated using the combined TMI and TRMM precipitation radar product (PR) and were then used to calibrate geosynchronous IR inputs (Huffman et al., 2007). The TRMM dataset covers a latitude range from 50°S to 50°N from 1998 to the present, and it is available at a 3-hourly temporal resolution in a 0.25-degree grid.

2.5. The combined scheme

The Combined Scheme (CoSch) was developed to include surface observations in satellite precipitation estimations; in this work, stations located along the border of Bolivia were also used. A short summary describing the technique of combining satellite and rain-gauge datasets is presented. Daily data represent a significant difficulty as compared with monthly data: the precipitation variability is larger over short periods than over long periods (monthly): therefore, CoSch calculated two types of bias: an additive bias and a ratio bias. The additive bias is calculated as follows:

$$rr^+ = rr_{sat} + \left(\overline{rr_{obs}^i - rr_{sat}^i}\right) \tag{1}$$

where rr_{sat} represents multi-satellite-based retrieval and $rr_{obs}^i - rr_{sat}^i$ represents the result of gridding (represented by the bar) the additive bias in the observed rainfall and satellite retrieval (TRMM3B42 in this case) at each station (denoted by the superscript i).

The ratio or multiplicative bias is calculated as follows:

$$rr^* = rr_{sat} \times \left(\overline{\frac{rr_{obs}^i}{rr_{sat}^i}}\right) \tag{2}$$

where the same conventions as in Eq. (1) were used.

The station-based biases are gridded using an inverse-distance-weighted algorithm (with controls) to fit the multi-satellite estimate resolution. All regions with a distance greater than five grid points from the closest station were masked (the grid size was set to 0.25° to match the satellite estimates). Despite precipitation estimation being height dependent and there are other factors such as slope, and slope orientation that may affect CoSch performance (Dinku et al., 2008), no topographic considerations were made to calculate these two biases.

The bias-corrected rainfall for the remaining terrestrial areas was defined as a weighted average of the additive and multiplicative bias-correction schemes as follows:

$$rrcorr_i = \alpha \times rr_i^+ + \beta \times rr_i^* \tag{3}$$

where $rrcorr_i$ is the final result of CoSch. Here, rr^+ and rr^* are defined in Eqs. (1) and (2) (the subscript i denotes a particular grid point), and α and β are weighting factors. These weighting factors represent the number of times a particular scheme is selected in a 3° × 3° box centered in the grid, in which i is divided by the total grid points in that particular box. $\alpha + \beta = 1$ for every non-masked grid point. This approach accounts for large-scale variations (the scheme works better over a larger area than a single grid point) and produces spatially continuous rainfall fields.
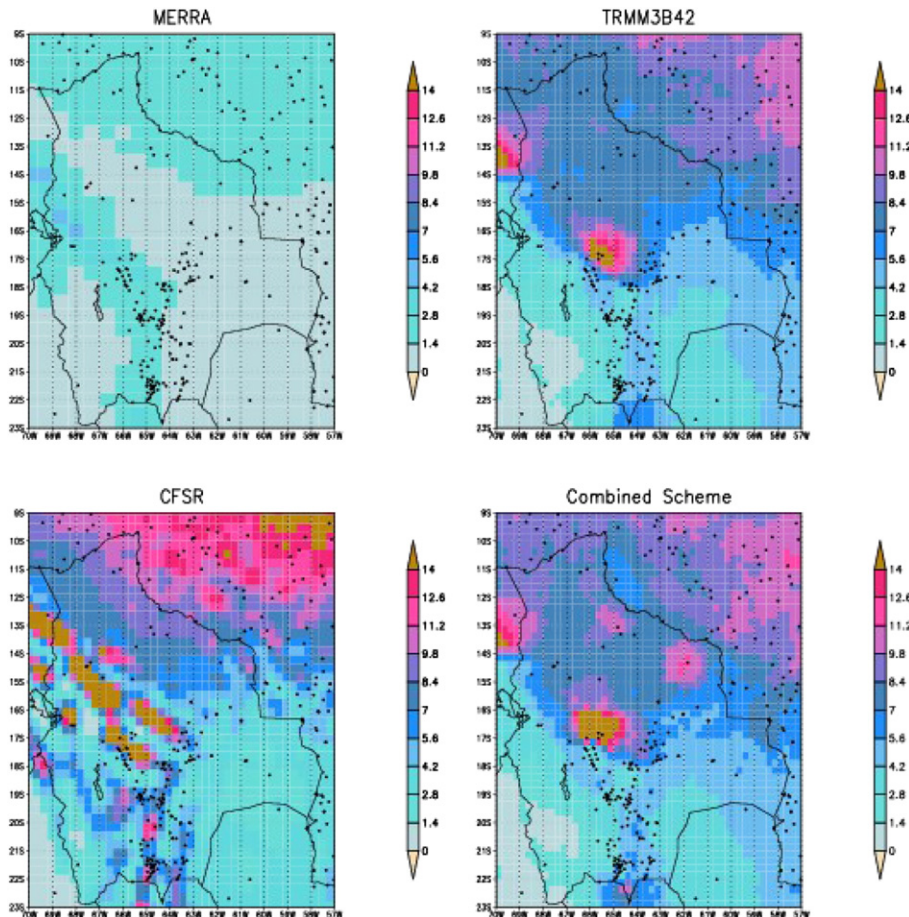

Fig. 3. Spatial rainfall distribution for DJF 1999–2009 in mm/day.

3. Results and discussion

3.1. Bolivia climatology

This section describes the precipitation climatology over Bolivia as obtained from the rain-gauge network and four datasets. The average daily precipitation rate corresponding to each month was calculated over 1999–2009 to describe the annual mean cycle. Next, the spatial distribution of the precipitation based on each product was presented and compared. Finally, the probability density functions were calculated for six precipitation classes: 0–1 mm/day, 1–3 mm/day, 3–10 mm/day, 10–20 mm/day, 20–50 mm/day, and >50 mm/day. Two types of probability density functions are presented: first, a population-based function that simply counts the number of occurrences for each class; and second, a volumetric analysis to calculate the total amount of precipitation in each class.

The annual precipitation cycle is monomodal, with a rainy season occurring in December–February and a dry season occurring in June–August (Fig. 2). There is a clear contrast between the La Plata and Altiplano basins as compared with the Amazon basin, during dry season rainfall is very scarce. During the onset months (September–November), a rapid monthly accumulation can also be observed over La Plata and Amazon basins.

CFSR and MERRA overestimated the precipitation over the Altiplano and La Plata basins each month. Over the Amazon basin, CFSR overestimated the precipitation during the rainy season, whereas MERRA better represented the annual cycle of precipitation. TRMM3B42 and CoSch performed well for all three basins, although TRMM3B42 exhibited a wet bias over the Altiplano basin during the dry season.

The Altiplano basin receives little precipitation throughout the year, as shown by TRMM3B42 and CoSch. However, while CFSR and MERRA represented the annual cycle qualitatively well, MERRA overestimated the precipitation every month, and CFSR overestimated the precipitation during the rainy season. The steep orographic gradients make this region complex for both reanalysis datasets.

Over the La Plata basin, all four precipitation estimates followed an annual cycle. CFSR and MERRA exhibited a wet bias in all months, and the overestimation was exacerbated during the onset months (September–November); however, TRMM3B42 and CoSch closely followed the rain gauges.

The Amazon basin was probably the best-represented region. CFSR had a tendency to overestimate precipitation during the rainy season months; however, all four estimates converged to similar values during the dry season.

The average daily precipitation was calculated for the rainy and dry seasons (Figs. 3 and 4, respectively) to study the spatially distributed precipitation described in MERRA, CFSR, TRMM3B42 and CoSch. In general, the geomorphological characteristics establish the spatial characteristics of precipitation: the lowlands on the eastern side of the Andes receive more precipitation than the highlands. The presence of the Andes generates orographic ascent on the eastern-facing slopes; on the western side, the moisture is prevented from reaching the Altiplano. Thus, a large contrast exists between the regions (Vuille and Keimig, 2004; Roche et al., 1990). Orographic precipitation is present over the eastern Cordillera (Cordillera Real, close to the Amazon) due to the moisture transport from the low-level jet (Vera et al., 2006). The northwest–southeast orientation of the Andes changes abruptly from the north–south orientation at 64°W–17°S; this feature modifies the moisture distribution: moisture is channeled to southeastern South America;
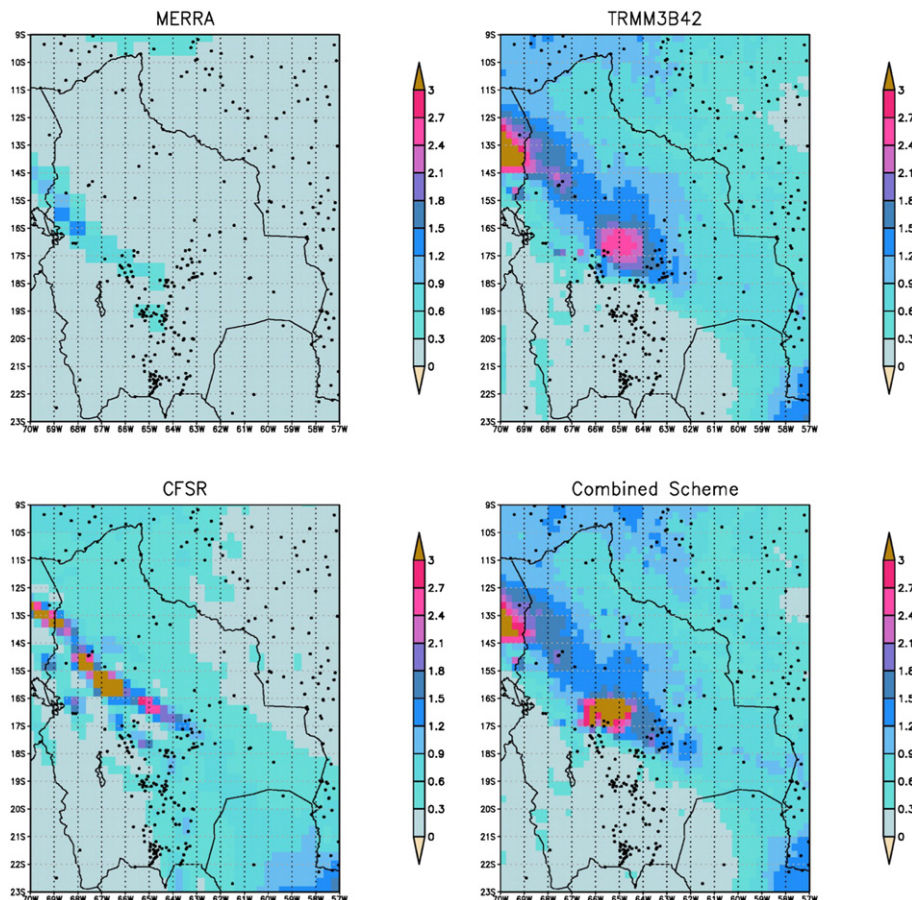

Fig. 4. Spatial rainfall distribution for JJA 1999–2009 in mm/day.

however, this phenomenon generates a "moisture supply shadow" that blocks the moisture influx and produces a very arid region called the Chaco, which is located along the border of Bolivia and Paraguay (see Fig. 1). Chaco region together with southern Altiplano constitute the driest regions over Bolivia.

In general, all four products correctly depicted broadly the spatial distribution of precipitation a very wet rainy season and a very dry season (Fig. 3). Precipitation along the northeastern-facing slopes of the Andes is greater than that over the rest of Bolivia. Two dry regions are evident: the Altiplano and Chaco regions. However, some differences
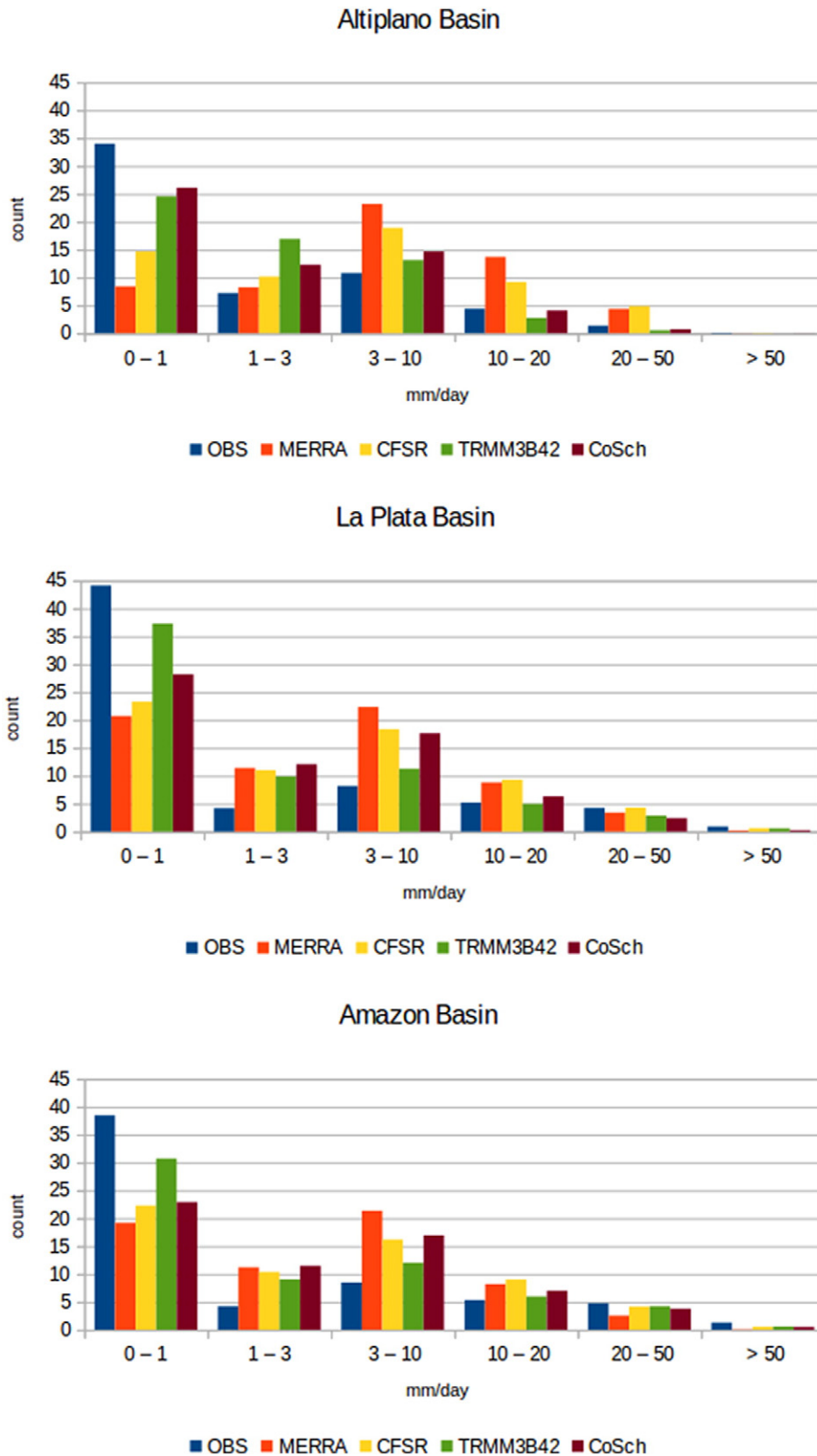

Fig. 5. Probability density function by population for DJF.

arise when comparing each product. During the rainy season (Fig. 3), MERRA broadly represented the difference between the wet north–northeastern (Amazon) and the dry southeastern (Chaco) regions; furthermore, the highest amounts of precipitation occurred on the Andes' eastern-facing slopes and near Titicaca Lake. Over the Altiplano, a north–south precipitation gradient occurred. However, the difference

between the Altiplano and Amazon precipitations was not well represented; furthermore, the spatial extent of dryness near the Chaco region was exaggerated. The east–west gradient over the Altiplano is only represented over the southern Altiplano. A possible cause of these inaccuracies is that MERRA's precipitation estimates do not benefit from the assimilation of surface rain-gauge data; instead, the onset, intensity,
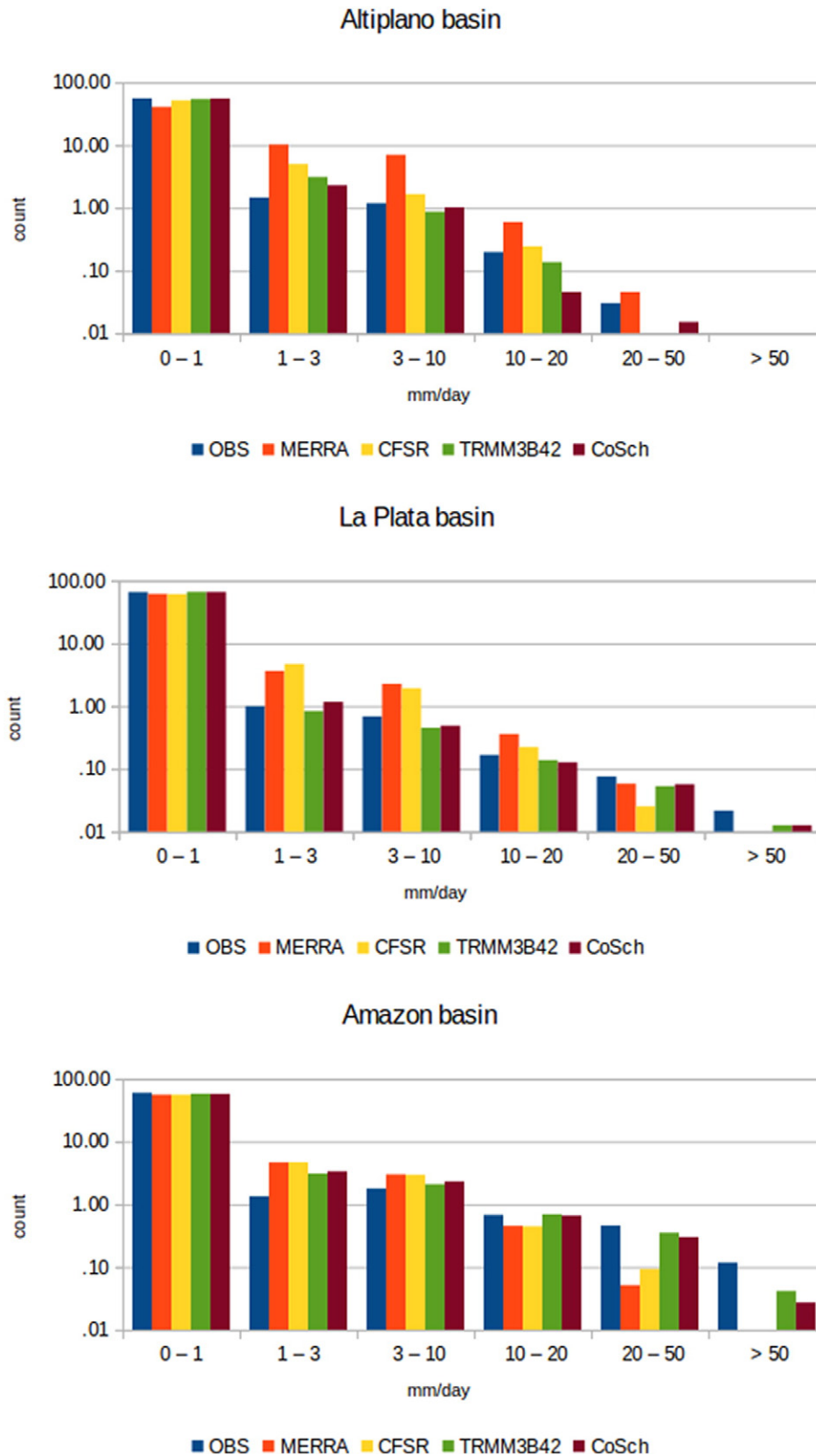

Fig. 6. Probability density function by population for JJA. The vertical scale is logarithmic.

and cessation of any rainfall event is mainly controlled by the model parameterizations (Rienecker et al., 2011; Reichle et al., 2011).

The general pattern depicted by CFSR was representative of the actual conditions. The Amazon region received more precipitation than the Altiplano and Chaco regions. CFSR had a tendency to overestimate precipitation over the Andes' eastern-facing slopes. Moreover, a double precipitation maximum is depicted between 16°S–18°S and 64°W–66°W. Over the Altiplano, CFSR exhibited a diverse precipitation pattern with no clear east–west or north–south gradient. Similar amounts of precipitation occurred in the southwestern Altiplano and eastern Amazonia. Over the southern rim of the Andes, CFSR also depicted increased precipitation; similar results have already been found (Silva et al., 2011). The
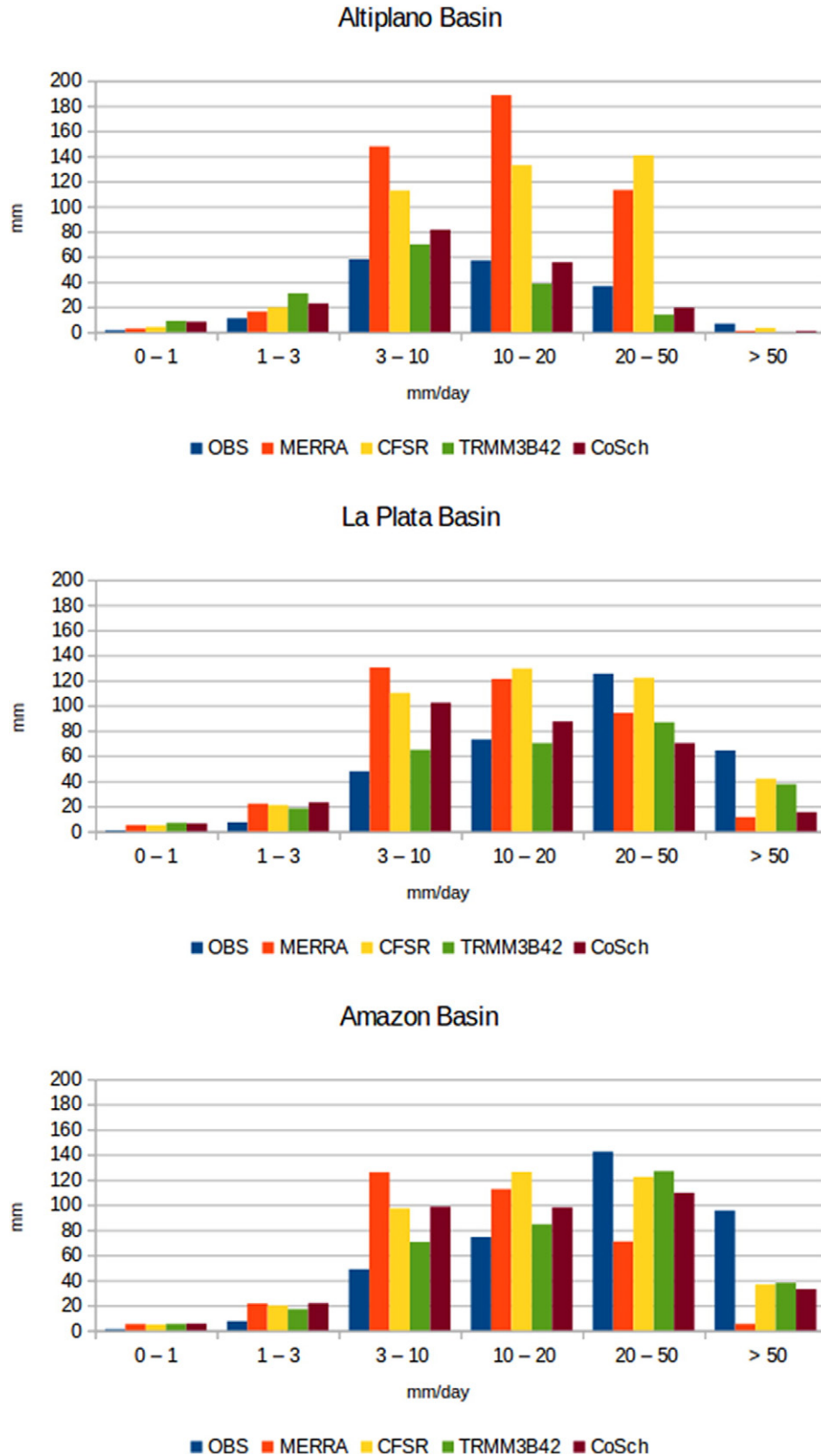

Fig. 7. Probability density function by volume for DJF.

double maximum and the overestimation might be related to the fact that CFSR relies upon surface observations and model-derived analyses that depend on satellite measurements. Over this particular region, there are few surface stations; therefore, the overestimation might be related to the satellite algorithm for estimating precipitation and to the CFSR's model parameterizations. This double maximum deserves further research.

The spatial patterns depicted by TRMM3B42 and CoSch resemble the known precipitation regime in the rainy season. The regions over the eastern lowlands received more precipitation than the highlands. Over the highlands, a north–south precipitation gradient occurred. Additionally, the Cordillera Real received more precipitation than the western Cordillera, i.e., an east–west precipitation gradient was present. The
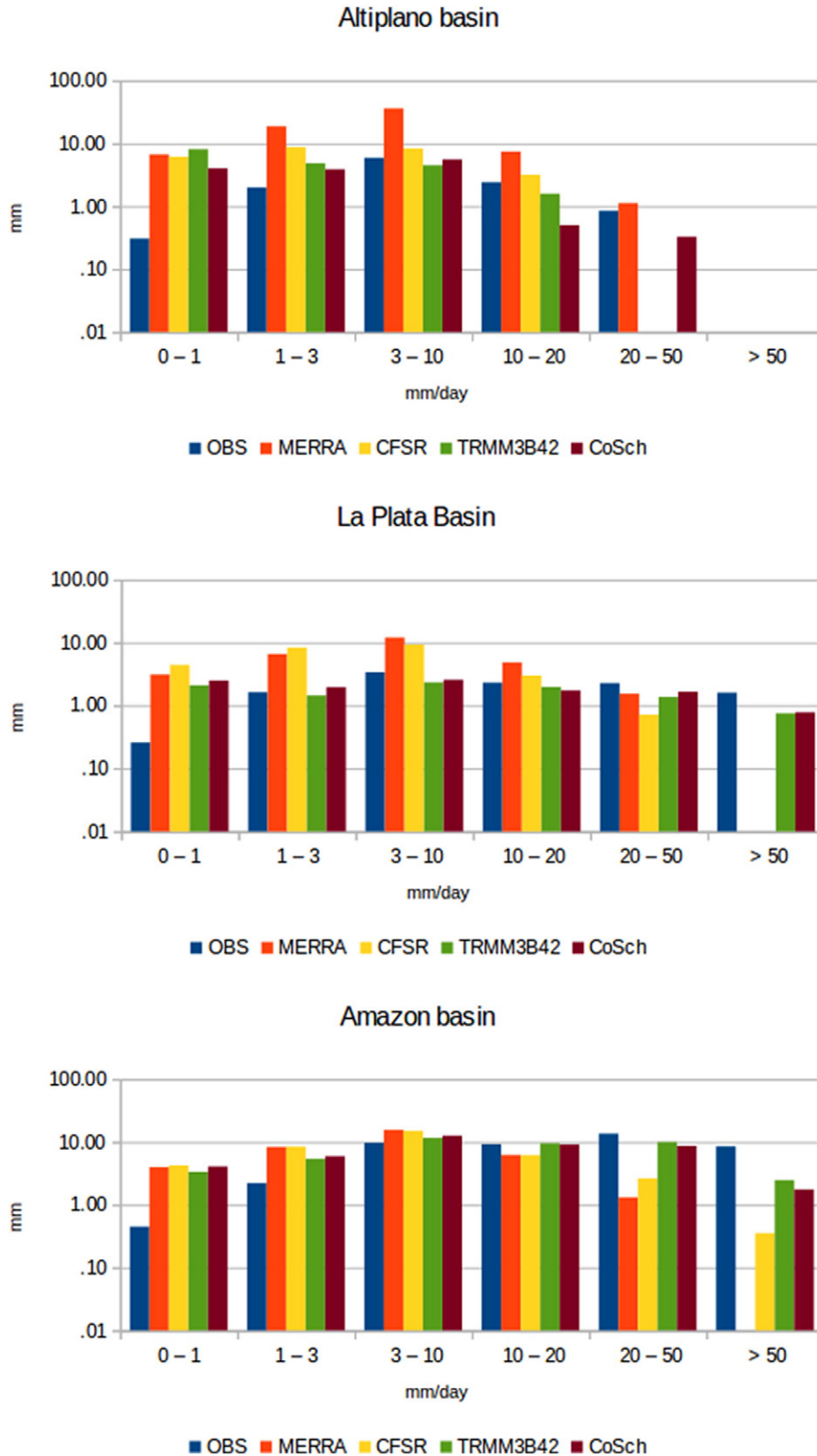

Fig. 8. Probability density function by volume for JJA. The vertical scale is logarithmic.

Table 2
Categorical statistics DJF.

	Altiplano basin				La Plata basin				Amazon basin			
	MERRA	CFSR	TRMM 3B42	CoSch	MERRA	CFSR	TRMM 3B42	CoSch	MERRA	CFSR	TRMM 3B42	CoSch
Accuracy	0.36	0.41	0.41	**0.42**	0.35	0.42	**0.49**	0.47	0.40	0.47	**0.53**	0.52
Bias frequency	2.82	2.65	**2.62**	2.65	2.90	2.61	**2.23**	2.52	2.49	2.21	**1.91**	2.19
POD	**1.00**	0.98	0.97	**1.00**	**1.00**	0.96	0.87	0.99	**1.00**	0.95	0.87	0.99
FAR	0.65	0.63	0.63	**0.62**	0.66	0.63	**0.61**	**0.61**	0.60	0.57	**0.54**	0.55
ETS	0.0018	0.0281	0.0300	**0.0388**	0.0007	0.0378	0.0676	**0.0727**	0.0004	0.0432	0.0837	**0.0878**

The bold values are the maximum/minimum corresponding to each statistical category when comparing the four datasets for each basin.

Chaco region received little precipitation. The maximum precipitation occurred in the Chapare region, which is located at 65.5°W–17.5°W (Roche et al., 1990).

Although CoSch broadly depicted the same features as TRMM3B42, differences were apparent over the Altiplano region: the northeast–southwest precipitation gradient was displaced to the southeast, i.e., the western-facing rim of the Cordillera Real received more precipitation than estimated by TRMM3B42. Similarly, over the southern Altiplano, CoSch indicated more precipitation than TRMM3B42. TRMM3B42 might be affected by warm rain processes, on the eastern facing slopes some of the systems can generate precipitating systems that may not be detected (Dinku et al., 2008). The precipitation maximum over the Chapare region was intensified and more clearly depicted, and the presence of three stations allowed us to confirm that the values are real and not artifacts of the algorithm; however, the spatial extent of the maximum is exaggerated probably due to the interpolation process, i.e., it renders homogeneity in the surface observation data over a relatively large region without accounting for the topography.

During the dry season (Fig. 4), MERRA exhibited a generally dry spatial pattern, with the exception of the northern Andes near Titicaca Lake. When comparing the results of the other three products, the largest precipitation rate was found for MERRA over this particular region. CFSR overestimated the precipitation along the Andes, but the Altiplano as a whole is dry (with the exception of the region near Titicaca Lake), and the Amazon and La Plata basins receive little precipitation.

TRMM3B42 and CoSch depicted Bolivia as two regions: the northeastern region and the southwestern region. The northeastern region received relatively more precipitation than the southwestern region. Over the northeastern region, the presence of a northeast–southwest precipitation gradient was exhibited; and a maximum occurred over the Chapare region.

Although differences exist among these products, the absolute differences are small due to the low precipitation amount in the dry season.

3.1.1. Probability density functions

Two types of probability density functions were calculated for the rainy and dry seasons for each basin (the Altiplano, La Plata, and Amazon basins) by constructing six precipitation classes (see Figs. 5 and 6). The first analysis was based on the population function, the second analysis was based on the cumulative rainfall for each class (Li et al., 2013).

When calculating the probability density function based on the population (see Fig. 5), the population was dominated by small systems (0–1 mm/day) in the rainy season (DJF). Nevertheless, in general, all four estimates follow the rain gauge behavior; all of the datasets underestimated the number of these systems (which will have little impact when calculating the amount of rainfall from these systems). CFSR and MERRA tended to overestimate the number of systems corresponding to 1–3, 3–10, and 10–20 mm/day; over the Altiplano, the previously discussed overestimation included the 20–50 mm/day class. TRMM3B42 and CoSch overestimated the 1–3 and 3–10 mm/day classes; however, they closely represented the 10–20 and 20–50 mm/day classes, which accounted for significant amounts of rainfall which was also found over Poyang Lake (Li et al., 2013).

Over the La Plata and Amazon basins, the behavior was very similar: the 0–1 mm/day class was underestimated by all estimates, while the 1–3, 3–10, and 10–20 mm/day classes were overestimated by all products. The 20–50 mm/day class was well represented by all of the datasets. This particular class contributed significantly to the precipitation, as seen in Fig. 7.

During the dry season (JJA, see Fig. 6), due to a lack of moisture and limited convective energy, the number and intensity of the systems was drastically reduced. The population was completely dominated by the 0–1 mm/day class in all three of the basins; this was the only class that was underestimated by all of the products in all three of the basins. Similar to DJF, over the La Plata and Amazon basins, all of the products overestimated the 1–3, 3–10, and 10–20 mm/day classes. Furthermore, for both basins, the 20–50 mm/day class was well represented by all of the datasets.

When calculating the amount of rainfall in each class, the results changed (see Figs. 7 and 8). During the rainy season, the 3–10, 10–20, and 20–50 mm/day classes contributed significantly to the total rainfall. The Amazon and La Plata basins received large amounts of rainfall in the 10–20, 20–50, and >50 mm/day classes, whereas in the Altiplano, the major contributors were systems corresponding to 3–10, 10–20, and 20–50 mm/day classes. The impact of the >50 mm/day class was different between the Altiplano and the La Plata and Amazon basins. Over the La Plata and Amazon basins, the contribution of this class was significant; in the Altiplano, this class played a limited role, and its contribution was even smaller than that of the 1–3 mm/day class. All of the datasets overestimated the 3–10 and 10–20 mm/day classes.

Table 3
Categorical statistics JJA.

	Altiplano basin				La Plata basin				Amazon basin			
	MERRA	CFSR	TRMM 3B42	CoSch	MERRA	CFSR	TRMM 3B42	CoSch	MERRA	CFSR	TRMM 3B42	CoSch
Accuracy	0.22	0.40	**0.18**	**0.18**	0.30	**0.64**	**0.64**	0.63	0.34	0.63	**0.59**	0.58
Bias frequency	11.21	**8.69**	11.65	11.66	11.63	**5.84**	5.89	6.65	24.49	**13.78**	15.12	16.14
POD	0.99	0.94	0.99	**1.00**	0.95	0.70	0.71	**0.97**	0.88	0.75	0.61	**0.94**
FAR	0.91	**0.89**	0.92	0.91	0.92	0.88	0.88	**0.85**	0.96	0.95	0.96	**0.94**
ETS	0.0127	**0.0335**	0.0091	0.0101	0.0173	0.0548	0.0568	**0.0860**	0.0084	0.0272	0.0124	**0.0312**

The bold values are the maximum/minimum corresponding to each statistical category when comparing the four datasets for each basin.
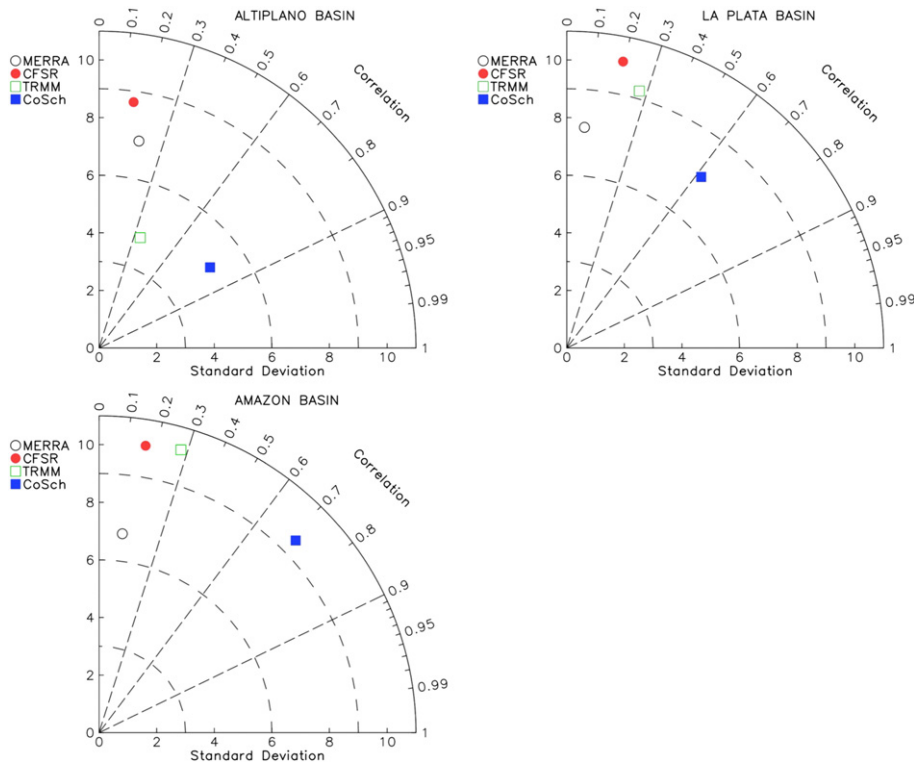
Fig. 9. Taylor diagram for rainy season (DJF) for the three basins.

Additionally, the 20–50 mm/day class in the Amazon and La Plata basins was underestimated by MERRA and CFSR. Over the Altiplano, both datasets overestimated the precipitation. Similar results were found for TRMM3B42 in the Poyang Lake basin (Li et al., 2013).

In the dry season (JJA, see Fig. 8), each basin behaved differently. Although all of the products overestimated the rainfall for each class over the Altiplano, MERRA exhibited the largest overestimation. CFSR, TRMM3B42, and CoSch behaved reasonably well regarding the 3–10, 10–20, and 20–50 mm/day classes, which were coincidently the classes that contributed the most to the total rainfall.

Over the La Plata basin, MERRA and CFSR overestimated the 0–1 mm/day to 10–20 mm/day classes, and it underestimated the
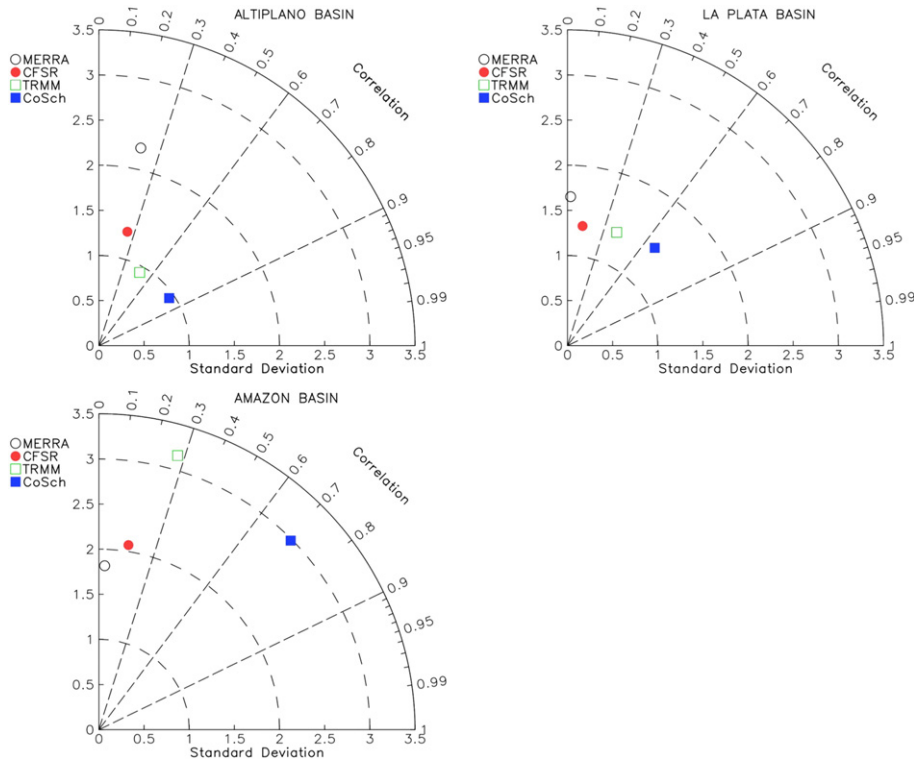

Fig. 10. Taylor diagram for dry season (JJA) for the three basins.

Table 4
Quantitative analysis DJF.

	Altiplano basin					La Plata basin					Amazon basin				
	OBS	MERRA	CFSR	TRMM 3B42	CoSch	OBS	MERRA	CFSR	TRMM 3B42	CoSch	OBS	MERRA	CFSR	TRMM 3B42	CoSch
Average	2.94	8.10	7.13	2.79	3.25	4.76	5.74	6.42	4.25	4.55	5.90	5.45	6.50	5.46	5.85
Stdev	6.03	7.32	8.62	4.09	4.76	11.49	7.69	10.14	9.27	7.55	13.73	6.96	10.09	10.22	9.55
Bias		−5.16	−4.19	**0.15**	−0.31		−0.99	−1.66	0.51	**0.21**		0.45	−0.60	0.44	**0.05**
RMSE		5.73	5.04	**1.97**	2.30		4.06	4.54	**3.00**	3.22		3.85	4.60	**3.86**	4.14

The bold values are the maximum/minimum corresponding to each statistical category when comparing the four datasets for each basin.

20–50 mm/day class. Heavy rainfall in the >50 mm/day systems was completely missed by CFSR and MERRA. TRMM3B42 and CoSch performed reasonably well in all of the precipitation classes, with the exception of the 0–1 mm/day class, which both datasets overestimated.

The precipitation behavior of the Amazon basin was mixed. The major contributors to the total rainfall were the 3–10 mm/day to >50 mm/day classes. MERRA and CFSR overestimated the 0–1 mm/day to 3–10 mm/day classes and underestimated the 10–20 mm/day to >50 mm/day classes. In fact, MERRA completely missed heavy rainfall systems, which contributed a non-negligible amount to the total rainfall. Although TRMM3B42 and CoSch performed relatively well compared with MERRA and CFSR, both underestimated the precipitation in the 20–50 mm/day and >50 mm/day classes.

In summary, it appears that the overestimation and underestimation are related to the same precipitation classes that represent much of the rain over the three basins, which include the 3–10, 10–20, and 20–50 mm/day classes.

During DJF over the La Plata and Amazon basins, MERRA and CFSR overestimated the 3–10 and 10–20 mm/day classes regarding both the population and volume (over the Altiplano basin, the CFSR overestimation included the 20–50 mm/day class). However, MERRA and CFSR underestimated the heavy rainfall class (>50 mm/day) regarding both the population and volume. TRMM3B42 and CoSch compensated for the total rainfall by slightly overestimating the 0–1 mm/day class and underestimating the 3–10 mm/day class.

During JJA, the behavior was similar, i.e., the systems that bring the largest amount of rain are key to understanding the datasets' overestimations/underestimations, such as those in the Altiplano basin. The MERRA overestimation (cf. Fig. 2 and Figs. 6 and 8) and CFSR underestimation might be related to errors in the 20–50 mm/day class. Very little precipitation occurs in the austral winter; thus, heavy precipitation systems are scarce; however, these systems cause significant amounts of rainfall that MERRA was not able to capture (see Figs. 6 and 8). MERRA's overestimation might be partially explained by its assimilation system, which presents difficulties related to tropical continental precipitation because of the reduced number of ground observations. The retrievals over land can also be complicated by cloudy conditions, and land–atmosphere interactions are challenging to parameterize (Bosilovich et al., 2008).

3.2. Statistical analysis

Two types of statistical analyses were performed. First, a categorical analysis that included calculations of accuracy, bias frequency,

probability of detection (POD), false alarm ratio (FAR), and an equitable threat score (ETS) for each basin and season (DJF and JJA) were made. Next, a quantitative analysis was performed by calculating the following parameters: the average (in mm/day), standard deviation (in mm/day), correlation coefficient, and root mean square error (RMSE, in mm/day).

3.2.1. Categorical analysis

During DJF over the three basins, the accuracy values were rather similar for the four products (see Table 2). Basically, the same behavior was depicted for the bias frequency, POD, and FAR indexes. The POD values were very high meaning that all databases were able to detect precipitation, however, the FAR values were also relatively high, which means that the products exhibit the tendency to detect spurious events. Despite that the accuracy values were similar, MERRA scores lowest for the three basins. CoSch systematically scores below TRMM3B42 for La Plata and Amazon basins. Differences arise when looking at the ETS: MERRA scores very low, TRMM3B42 and CFSR score similarly, and CoSch scores slightly above the other three.

During the dry season (JJA, see Table 3), despite the similarities in the accuracy, bias frequency, POD, and FAR values, a separate analysis was conducted. For the Altiplano basin, it can be noted that the CFSR accuracy outperformed the other three products; furthermore, the dataset had the lowest bias frequency. Although the POD and FAR values were rather similar, the ETS presented a difference, and CRSR outperformed the other products. For the La Plata and Amazon basins, the behavior was similar, particularly for the POD and FAR values. However, MERRA scored low on accuracy and scored very high on bias frequency. Notably, CoSch's accuracy values were lower than those for TRMM3B42 and CFSR. Moreover, CoSch's bias frequency score was larger than that for TRMM3B42 and CFSR. In contrast to all of the aforementioned values, CoSch and CFSR presented the highest ETS values, with the exception of the Altiplano, where MERRA and CFSR scored the highest.

3.2.2. Quantitative analysis

A quantitative analysis was performed by calculating the average, bias, standard deviation, correlation coefficient, and RMSE parameters. Taylor diagrams were plotted (Taylor, 2001) for each season to compare the correlation coefficients and the standard deviations (see Figs. 9 and 10). For the other parameters, a table for each season was prepared (see Tables 4 and 5). Each table lists the average, standard deviation, bias, and RMSE values. Caution should be exercised when analyzing the bias because the values can be positive or negative; when the total sum is calculated, the negative and positive biases could cancel out. To

Table 5
Quantitative analysis JJA.

	Altiplano basin					La Plata basin					Amazon basin				
	OBS	MERRA	CFSR	TRMM 3B42	CoSch	OBS	MERRA	CFSR	TRMM 3B42	CoSch	OBS	MERRA	CFSR	TRMM 3B42	CoSch
Average	0.20	1.20	0.45	0.33	0.25	0.17	0.42	0.38	0.15	0.16	0.68	0.55	0.57	0.66	0.65
Stdev	1.24	2.24	1.30	0.93	0.94	1.93	1.65	1.34	1.37	1.45	4.46	1.82	2.07	3.16	2.98
Bias		−1.01	−0.25	−0.13	**−0.05**		−0.25	−0.21	0.02	**0.00**		0.13	0.11	**0.02**	0.02
RMSE		0.85	0.32	0.23	**0.17**		0.29	0.27	**0.10**	0.12		**0.39**	0.41	0.47	0.46

The bold values are the maximum/minimum corresponding to each statistical category when comparing the four datasets for each basin.

consider the differences, the RMSE must be calculated and both parameters should be analyzed together.

3.2.2.1. Taylor diagram analyses. Two Taylor diagram sets were generated. Fig. 9 corresponds to the austral summer, and Fig. 10 corresponds to the austral winter. For the rainy season (DJF, Fig. 9), the correlation values from MERRA, CFSR, and TRMM3B42 scored low, as also found by Li et al. (2013). However, the correlation coefficients for CoSch were the highest for each basin ($r > 0.6$). The highest value was found in the Altiplano ($r = 0.81$), and the lowest value was found in the La Plata basin ($r = 0.62$). In the dry season (JJA, Fig. 10), the correlation values for MERRA, CFSR, and TRMM3B42 scored low. However, CoSch's correlation coefficients were the highest for each basin. Similarly to the rainy season, CoSch's correlation coefficients were rather high ($r > 0.6$); the highest value was found for the Altiplano ($r = 0.83$), and the lowest value was found for the La Plata basin ($r = 0.67$).

The average, bias, and RMSE values were analyzed. CFSR and MERRA depicted a wet bias over the Altiplano and La Plata basins in both seasons (see Tables 4 and 5). However, the bias values for TRMM3B42 and CoSch scored low. Overall, the RMSE values were larger during DJF than during JJA, probably due to the large and variable amounts of precipitation that fall during the austral summer in the three basins. Over the Altiplano and La Plata basins, the RMSE exhibited a similar behavior: MERRA and CRSR presented the largest values and TRMM and CoSch presented the smallest values in both seasons. In contrast, the RMSE values over the Amazon basin were rather similar. The Altiplano basin presents a major challenge for CFSR and MERRA reanalysis data.

4. Conclusions

A precipitation comparison of two reanalysis datasets (the CFSR and MERRA), a satellite estimation algorithm (TRMM3B42), and a combined product (TRMM3B42 + observations) was performed for the rainy and dry seasons during 1999–2009 over three major basins in Bolivia: the Altiplano, La Plata, and the Amazon.

All of the datasets were able to depict the annual precipitation cycles. CFSR and MERRA overestimated the precipitation, particularly over the Altiplano basin. All of the datasets depicted broadly similar spatial distributions; i.e., the Altiplano and the Andes received less precipitation compared with the Amazon region, and the Chaco region had the lowest amount of precipitation. However, differences were also apparent. MERRA broadly represented the difference in the rainfall amounts between the Bolivian Amazon basin and the Altiplano, while it overestimated the precipitation over the Andes' northeastern-facing slopes. CFSR overestimated the precipitation over the Andes' northeastern-facing slopes during DJF, where a double precipitation maximum occurred (16°S to 18°S) (Silva et al., 2011; Eichler and Londoño, 2013); this finding deserves further research.

TRMM3B42 underestimated the precipitation in two regions: the western-facing rim of the Cordillera Real and the southern Altiplano. Furthermore, CoSch exaggerated the spatial extent of the precipitation maximum over the Chapare because of the interpolation process (Vila et al., 2009). At the same time, TRMM3B42 and CoSch exhibit underestimated heavy rainfall (>50 mm/day) on both rainy and dry seasons. These results are in reasonable agreement with studies conducted in the region but for a different period (Andrade, 2014).

The precipitation classes that contributed the most to the total rainfall were a key to understanding each dataset's overestimations/underestimations, as also shown by Li et al. (2013). The 3–10 and 10–20 mm/day classes partially explained the MERRA overestimations in the Altiplano basin and underestimations in the Amazon basin. The same precipitation rates explained CFSR's overestimation in all three of the basins.

When comparing the bias, RMSE, and correlation coefficients, CoSch outperformed CFSR, MERRA, and TRMM3B42. Despite the generally low ETS score, it was possible to distinguish between all four products:

CoSch outperformed all of the other products, followed by TRMM3B42, CFSR, and MERRA.

Overall, the outcome of combining TRMM3B42 with the surface observations is positive, and the spatial and statistical satellite representations were improved. Thus, we are confident that the gridded dataset can be used for future applications. To improve the knowledge of the biases and errors in the different products, the topographic dependence, such the height, slope, and slope orientation, must be explored in relation to the wind direction and daily rainfall.

References

Andrade, M., 2014. Generación de datos meteorológicos de alta resolución para Bolivia in La economía del cambio climático en Bolivia. Inter-American Development Brank Climate Change and Sustainability Division, Series IDB-MG-200.

Arkin, P.A., Meisner, B.N., 1987. The relationship between large-scale convective rainfall and cold cloud over the western hemisphere during 1982–84. Mon. Weather Rev. 115, 51–74.

Behrangi, A., Khakbaz, B., Jaw, T.C., AghaKouchak, A., Hsu, K., Sorooshian, S., 2011. Hydrologic evaluation of satellite precipitation products over a mid-size basin. J. Hydrol. 397, 225–237. http://dx.doi.org/10.1016/j.jhydrol.2010.11.043.

Bosilovich, M.G., Chen, J., Robertson, F.R., Adler, R.F., 2008. Evaluation of global precipitation in reanalyses. J. Appl. Meteorol. Climatol. 47, 2279–2299. http://dx.doi.org/10.1175/2008JAMC1921.1.

Carvalho, L.M.V., Jones, C., Posadas, A.N.D., Quiroz, R., Bookhagen, B.M.V., Liebmann, B., 2012. Precipitation characteristics of the South American Monsoon System derived from multiple data sets. J. Clim. 25, 4600–4620. http://dx.doi.org/10.1175/JCLI-D-11-00335.1.

Clarke, R.T., Buarque, D.C., de Paiva, R.C.D., Collischonn, W., 2011. Issues of spatial correlation arising from the use of TRMM rainfall estimates in the Brazilian Amazon. Water Resour. Res. 47, W05539. http://dx.doi.org/10.1029/2010WR010334.

De Gonçalves, L.G.G., Shuttleworth, W.J., Nijssen, B., Burke, E.J., Marengo, J.A., Chou, S.C., Houser, P.R., Toll, D.L., 2006. Evaluation of model-derived and remotely sensed precipitation products for continental South America. J. Geophys. Res. 111. http://dx.doi.org/10.1029/2005JD006276 (http://dx.doi.org/10.1029/2005JD006276).

Dinku, T., Chidzambwa, S., Ceccato, P., Connor, S.J., Ropelewski, C.F., 2008. Validation of high-resolution satellite rainfall products over complex terrain. Int. J. Remote Sens. 29, 4097–4110. http://dx.doi.org/10.1080/01431160701772526.

Dinku, T., Connor, S.J., Ceccato, P., 2010. Comparison of CMORPH and TRMM-3B42 over mountainous regions of Africa and South America. In: Gebremichael, M., Hossain, F. (Eds.), Satel. Rainfall Appl. Surf. Hydrol. Springer, Verlag, pp. 193–204.

Ebert, E.E., Janowiak, J.E., Kidd, C., 2007. Comparison of near-real-time precipitation estimates from satellite observations and numerical models. Bull. Am. Meteorol. Soc. 88, 47–64. http://dx.doi.org/10.1175/BAMS-88-1-47.

Eichler, T.P., Londoño, A.C., 2013. South American climatology and impacts of El Niño in NCEP's CFSR data. Adv. Meteorol. 2013, 1–15.

Heidinger, H., Yarlequé, C.bi., Posadas, A.N.D., Quiroz, R., 2012. TRMM rainfall correction over the Andean plateau using wavelet multi-resolution analysis. Int. J. Remote Sens. 33, 4583–4602. http://dx.doi.org/10.1080/01431161.2011.652315 (http://www.tandfonline.com/doi/abs/10.1080/01431161.2011.652315).

Herdies, D.L., da Silva, A., Silva Dias, M.A.F., Nieto-Ferreira, R., 2002. Moisture budget of the bimodal pattern of the summer circulation over South America. J. Geophys. Res. 107, 1–10. http://dx.doi.org/10.1029/2001JD000997.

Hou, A.Y., et al., 2013. The Global Precipitation Measurement (GPM) mission. Bull. Am. Meteorol. Soc. http://dx.doi.org/10.1175/BAMS-D-13-00164.1 (130909112500001).

Huffman, G.J., Adler, R.F., Rudolf, B., Schneider, U., Keehn, P.R., 1995. Global precipitation estimates based on a technique for combining satellite-based estimates, rain gauge analysis, and NWP model precipitation information. J. Clim. 8, 1284–1295.

Huffman, G.J., Adler, R.F., Rudolf, B., Schneider, U., Keehn, P.R., 2007. The TRMM multisatellite precipitation analysis (TMPA): quasi-global, multiyear, combined-sensor precipitation estimates at fine scales. J. Hydrometeorol. 8, 38–55. http://dx.doi.org/10.1175/JHM560.1.

Johnson, R.H., Ciesielski, P.E., L'Ecuyer, T.S., Newman, A.J., 2010. Diurnal cycle of convection during the 2004 North American Monsoon Experiment. J. Clim. 23, 1060–1078. http://dx.doi.org/10.1175/2009JCLI3275.1.

Kummerow, C.D., Barnes, W., Kozu, T., Shiue, J., Simpson, J., 1998. The Tropical Rainfall Measuring Mission (TRMM) sensor package. J. Atmos. Ocean. Technol. 15, 809–817.

Lenters, J.D., Cook, K.H., 1997. On the origin of the Bolivian high and related circulation features of the South American climate. J. Atmos. Sci. 54, 656–678. http://dx.doi.org/10.1175/1520-0469(1997)054<0656:OTOOTB>2.0.CO;2.

Lenters, J.D., Cook, K.H., 1999. Summertime precipitation variability over South America: role of the large-scale circulation. Mon. Weather Rev. 127, 409–431.

Li, X., Zhang, Q., Xu, C.-Y., 2013. Assessing the performance of satellite-based precipitation products and its dependence on topography over Poyang lake basin. Theor. Appl. Climatol. http://dx.doi.org/10.1007/s00704-013-0917-x.

Liu, Z., Ostrenga, D., Teng, W., Kempler, S., 2012. Tropical Rainfall Measuring Mission (TRMM) precipitation data and services for research and applications. Bull. Am. Meteorol. Soc. 93.

Nespor, V., Sevruk, B., 1999. Estimation of wind-induced error of rainfall gauge measurements using a numerical simulation. J. Atmos. Ocean. Technol. 16, 450–464.

Nogués-Paegle, J., Mo, K.C., 1997. Alternating wet and dry conditions over South America during summer. Mon. Weather Rev. 125, 279–291. http://dx.doi.org/10.1175/1520-0493(1997)125<0279:AWADCO>2.0.CO;2.

Ouma, Y.O., Owiti, T., Kipkorir, E., Kibiiy, J., Tateishi, R., 2012. Multitemporal comparative analysis of TRMM-3B42 satellite-estimated rainfall with surface gauge data at basin scales: daily, decadal and monthly evaluations. Int. J. Remote Sens. 33, 7662–7684.

Porcù, F., Milani, L., Petracca, M., 2014. On the uncertainties in validating satellite instantaneous rainfall estimates with raingauge operational network. Atmos. Res. 144, 73–81. http://dx.doi.org/10.1016/j.atmosres.2013.12.007.

Quadro, M.F.L. de, da S. Dias, M.A.F., de Gonçalves, L.G.G., 2007. Avaliação do transporte de umidade e precipitação associada à ZCAS no verão do HS através da nova geração de reanálises. In: São Paulo, S.P. (Ed.), Proc. XV CBMET, S.B. Meteorol. CBMET.

Quadro, M.F.L. de, Herdies, D.L., de Gonçalves, L.G.G., 2012. Análise climatológica da precipitação e do transporte de umidade na região da ZCAS através da nova geração de reanálises. Rev. Bras. Meteorol. 27, 152–162.

Reichle, R.H., Koster, R.D., De Lannoy, G.J.M., Forman, B.A., Liu, Q., Mahanama, S.P.P., Touré, A., 2011. Assessment and enhancement of MERRA land surface hydrology estimates. J. Clim. 24, 6322–6338. http://dx.doi.org/10.1175/JCLI-D-10-05033.1.

Rienecker, M.M., et al., 2008. The GEOS-5 Data Assimilation System — Documentation of Versions 5.0.1,5.1.0, and 5.2.0.

Rienecker, M.M., et al., 2011. MERRA: NASA's modern-era retrospective analysis for research and applications. J. Clim. 24, 3624–3648. http://dx.doi.org/10.1175/JCLI-D-11-00015.1.

Roche, M.A., Aliaga, A., Campos, J., Peña, J., Cortés, J., Rocha, N., 1990. Hétérogénéité des précipitations sur la cordillère des Andes boliviennes. In: Lang, H., Musy, A. (Eds.), Hydrology in Mountainous Regions, 1- Hydrological Measurements; the Water Cycle. Lausanne, Switzerland, Int. Assoc. Hydrol. Sci. Publ. Vol. 193, pp. 381–388.

Rozante, J.R., Moreira, D.S., de Goncalves, L.G.G., Vila, D.A., 2010. Combining TRMM and surface observations of precipitation: technique and validation over South America. Weather Forecast. 25, 885–894. http://dx.doi.org/10.1175/2010WAF2222325.1.

Saha, S., et al., 2010. The NCEP climate forecast system reanalysis. Bull. Am. Meteorol. Soc. 91, 1015–1057. http://dx.doi.org/10.1175/2010BAMS3001.1.

Salio, P., Hobouchian, M.P., Skabar, Y.G., Vila, D., 2014. Evaluation of high-resolution satellite precipitation estimates over southern South America using a dense rain gauge network. Atmos. Res. http://dx.doi.org/10.1016/j.atmosres.2014.11.017 (http://www.sciencedirect.com/science/article/pii/S0169809514004219).

Silva, V.B.S., Kousky, V.E., Higgins, R.W., 2011. Daily precipitation statistics for South America: an intercomparison between NCEP reanalyses and observations. J. Hydrometeorol. 12, 101–117. http://dx.doi.org/10.1175/2010JHM1303.1.

Smith, E.A., et al., 2004. International Global Precipitation Measurement (GPM) Program and Mission: An Overview. Meas. Precip. From Sp. EURAINSAT Futur.

Spencer, R.W., GoodMan, H.M., Hood, R.E., 1989. Precipitation retrieval over land and ocean with the SSM/I: identification and characteristics of the scattering signal. J. Atmos. Ocean. Technol. 6, 254–273.

Tapiador, F.J., et al., 2012. Global Precipitation Measurement: methods, datasets and applications. Atmos. Res. 104–105, 70–97. http://dx.doi.org/10.1016/j.atmosres.2011.10.021.

Taylor, K.E., 2001. Summarizing multiple aspects of model performance in a single diagram. J. Geophys. Res. 106, 7183–7192. http://dx.doi.org/10.1029/2000JD900719.

Tian, Y., Peters-Lidard, C.D., 2010. A global map of uncertainties in satellite-based precipitation measurements. Geophys. Res. Lett. 37. http://dx.doi.org/10.1029/2010GL046008 L24407.

Treadon, R., Pan, H.-L., Wu, W.-S., Lin, Y., Olson, W.S., Kuligowski, R.J., 2002. Global and regional moisture analyses at NCEP. ECMWF/GEWEX Workshop on Humidity Analysis vol. 27 pp. 33–47.

Vila, D.A., de Gonçalves, L.G.G., Toll, D.L., Rozante, J.R., 2009. Statistical evaluation of combined daily gauge observations and rainfall satellite estimates over continental South America. J. Hydrometeorol. 10, 533–543. http://dx.doi.org/10.1175/2008JHM1048.1.

Vera, C., Baez, J., Douglas, M., Emmanuel, C.B., Marengo, J., Meitin, J., Nicolini, M., Nogues-Paegle, J., Paegle, J., Penalba, O., Salio, P., Saulo, C., Silva Dias, M.A., Silva Dias, P., Zipser, E., 2006. The South American Low-Level Jet Experiment. Bull. Am. Meteorol. Soc. 87, 63–77. http://dx.doi.org/10.1175/BAMS-87-1-63 http://journals.ametsoc.org/doi/abs/10.1175/BAMS-87-1-63.

Vuille, M.R., Keimig, F.R., 2004. Interannual Variability of Summertime Convective Cloudiness and Precipitation in the Central Andes Derived from ISCCP-B3 Data. J. Clim. 17, 3334–3348. http://dx.doi.org/10.1175/1520-0442(2004)017<3334:IVOSCC>2.0.CO;2.

Ward, E., Buytaert, W., Peaver, L., Wheater, H., 2011. Evaluation of precipitation products over complex mountainous terrain: a water resources perspective. Adv. Water Resour. 34, 1222–1231. http://dx.doi.org/10.1016/j.advwatres.2011.05.007.

Wilks, D.S., 2006. Statistical Methods in the Atmospheric Sciences. Elsevier (Second., p. 627).

Xie, P., Yatagai, A., Chen, M., Hayasaka, T., Fukushima, Y., Liu, C., Yang, S., 2007. A gauge-based analysis of daily precipitation over East Asia. J. Hydrometeorol. 8.

Yang, Y., Luo, Y., 2014. Evaluating the performance of remote sensing precipitation products CMORPH, PERSIANN, and TMPA, in the arid region of northwest China. Theor. Appl. Climatol. 1–17. http://dx.doi.org/10.1007/s00704-013-1072-0.

Zhao, C., Wang, J., Yao, S., Zhou, Z., 2012. A method for combined satellite and rain gauge of precipitation over Qinghai. 2nd International Conference on Remote Sensing, Environment and Transportation Engineering (RSETE), pp. 1–4.